Technobius Physics, 2026, 4(3), 0057, DOI: https://doi.org/10.54355/tbusphys/30070147.4.3.2026.0057

Technobius Physics

https://technobiusphysics.kz/

e-ISSN 3007-0147

Article

Structural disorder induced enhancement of dielectric energy storage performance in lead-free ceramics

Alexey Fedorov*

Electronic Ceramics Department, Jozef Stefan Institute, Ljubljana, Slovenia
*Correspondence: alexey.fedorov@ijs.si

Abstract. The development of lead-free dielectric ceramics with simultaneously high recoverable energy density, high energy-storage efficiency, and excellent operational stability remains a significant challenge for advanced electrostatic capacitors. In this work, the influence of controlled structural disorder on the structural evolution, dielectric response, polarization behavior, and energy-storage performance of lead-free ceramics was systematically investigated. Ceramic samples with different levels of compositional disorder were synthesized using a conventional solid-state reaction route and characterized by X-ray diffraction, field-emission scanning electron microscopy, dielectric spectroscopy, and polarization measurements under high electric fields. The results demonstrated that increasing structural disorder refined the grain structure, enhanced lattice distortion, and promoted the transition from normal ferroelectric to relaxor behavior. The optimized composition exhibited the highest maximum polarization of approximately 52 μC cm^{-2} together with a low remanent polarization of about 3 μC cm^{-2}, resulting in a recoverable polarization difference of nearly 49 μC cm^{-2}. Owing to the combined effects of improved polarization reversibility and enhanced dielectric breakdown strength approaching 480 kV cm^{-1}, a recoverable energy density of approximately 5.8 J cm^{-3} and an energy-storage efficiency close to 89% were achieved. Furthermore, the optimized ceramic maintained stable energy-storage characteristics over a wide temperature range and under different operating frequencies, indicating excellent thermal and frequency stability. These findings demonstrate that controlled structural disorder is an effective strategy for simultaneously optimizing polarization reversibility, dielectric breakdown strength, and dielectric energy-storage performance, providing a promising pathway for the design of high-performance lead-free dielectric ceramics for advanced pulse power and electrostatic energy-storage applications.

Keywords: lead-free ceramics, structural disorder, dielectric energy storage, relaxor ferroelectrics, polarization behavior, dielectric breakdown strength.

1. Introduction

The rapid development of renewable energy systems, electrified transportation, pulsed power technologies, and high-frequency power electronics has created an increasing demand for dielectric capacitors capable of operating under high electric fields while simultaneously delivering high power density, fast charge–discharge rates, and excellent long-term reliability [1], [2], [3]. Unlike electrochemical energy-storage systems, dielectric capacitors store energy through electrostatic polarization rather than electrochemical reactions, allowing energy release within microseconds and enabling exceptional cycling durability. These unique characteristics make dielectric capacitors indispensable components in advanced electronic devices, medical equipment, aerospace systems, electric vehicles, electromagnetic launch technologies, and modern power conversion circuits [1], [3].

The recoverable energy density of dielectric materials is fundamentally determined by both the polarization behavior and the maximum electric field that the material can withstand before dielectric breakdown occurs. Consequently, the development of advanced dielectric ceramics has increasingly focused on simultaneously maximizing induced polarization, minimizing remanent polarization, and improving dielectric breakdown strength. Achieving these three objectives

simultaneously remains a considerable scientific challenge because they are frequently governed by competing structural mechanisms. Conventional ferroelectric materials generally exhibit large spontaneous polarization; however, the irreversible switching of ferroelectric domains results in broad polarization hysteresis loops and considerable energy dissipation during charge–discharge cycles. Conversely, linear dielectric materials possess excellent efficiency but typically exhibit insufficient polarization for practical high-energy-density applications [3].

During the last decade, lead-free relaxor ferroelectric ceramics have emerged as one of the most promising classes of dielectric materials capable of overcoming this long-standing trade-off. Their polarization originates primarily from dynamic polar nanoregions rather than stable long-range ferroelectric domains, allowing large electric-field-induced polarization while maintaining comparatively low remanent polarization after removal of the external electric field [1], [2]. This reversible polarization process produces slim hysteresis loops and significantly increases the recoverable fraction of stored electrostatic energy. As environmental regulations continue to restrict the use of lead-containing electronic materials, the search for high-performance lead-free alternatives has become an important research direction in functional ceramics [2], [3].

Recent advances have demonstrated that the most significant improvements in dielectric energy-storage performance are no longer achieved solely through compositional optimization but rather through deliberate manipulation of local structural heterogeneity across multiple length scales. In particular, increasing attention has been devoted to engineering chemically disordered A-sites and B-sites, inducing lattice distortion, generating random electric fields, and controlling defect distributions in order to tailor polarization dynamics without sacrificing dielectric strength. These approaches have considerably expanded the design philosophy of lead-free dielectric ceramics from conventional phase-boundary engineering toward defect- and disorder-driven polarization engineering, which is currently regarded as one of the most promising strategies for achieving simultaneously high recoverable energy density and ultrahigh efficiency [4], [5], [6], [7], [8], [9], [10].

Unlike conventional compositional optimization, structural disorder engineering directly influences the local crystal potential by introducing random electric fields, lattice strain, and nanoscale chemical heterogeneity. These structural perturbations destabilize long-range ferroelectric domains while promoting the formation of dynamic polar nanoregions (PNRs), which possess considerably higher polarization reversibility than classical ferroelectric domains. Since PNRs continuously respond to external electric fields through reversible dipolar fluctuations instead of irreversible domain-wall switching, dielectric hysteresis is substantially reduced while maintaining relatively high induced polarization. Consequently, structural disorder provides an effective mechanism for simultaneously increasing recoverable energy density and energy-storage efficiency.

Another important consequence of structural disorder is the development of relaxor behavior. Unlike classical ferroelectrics, where the ferroelectric–paraelectric phase transition occurs abruptly at a well-defined Curie temperature, relaxor ferroelectrics exhibit diffuse dielectric maxima accompanied by strong frequency dispersion. Such behavior originates from nanoscale compositional heterogeneity and random local electric fields, which fragment long-range ferroelectric domains into dynamically fluctuating polar nanoregions [2], [11]. These nanoscale entities can rapidly align with an applied electric field while relaxing almost completely after field removal, producing the slim polarization hysteresis loops required for efficient dielectric energy storage. Consequently, the transition from classical ferroelectric behavior toward relaxor polarization dynamics has become one of the principal objectives in the design of modern lead-free dielectric ceramics.

It should be emphasized that lattice distortion and grain refinement contribute to dielectric energy-storage performance through fundamentally different physical mechanisms. Local lattice distortion primarily modifies intrinsic polarization dynamics by changing interatomic interactions and the stability of polar nanoregions, whereas grain refinement mainly influences the extrinsic electrical response by increasing the number of grain boundaries, interrupting conductive pathways, and reducing local electric-field concentration. Although these mechanisms frequently develop

simultaneously during compositional modification, distinguishing their individual contributions is essential for establishing reliable structure–property relationships and rational materials design.

Despite these considerable advances, establishing an optimal degree of structural disorder remains a challenging task. Excessively ordered materials generally retain stable ferroelectric domains, leading to high remanent polarization and significant hysteresis losses. In contrast, excessive disorder may weaken dipolar interactions to such an extent that the maximum attainable polarization decreases substantially, thereby reducing recoverable energy density despite improvements in efficiency. Therefore, structural disorder should not be regarded simply as a means of suppressing ferroelectricity; rather, it must be carefully controlled to achieve a balance between reversible polarization dynamics and sufficiently strong electric-field-induced polarization. Understanding this balance represents one of the central challenges in contemporary dielectric materials research.

Furthermore, recent investigations have demonstrated that relaxor behavior cannot be adequately characterized solely by diffuse dielectric maxima. Dynamic freezing of polar nanoregions, commonly described using the Vogel–Fulcher relationship, provides additional insight into the interaction strength between local dipoles and the evolution of polarization dynamics. Consequently, quantitative evaluation of dielectric relaxation parameters has become an important tool for correlating structural disorder with macroscopic dielectric performance. In the present work, this aspect is considered together with structural and polarization analyses to provide a more comprehensive understanding of the disorder-induced energy-storage mechanism.

The growing interest in structural disorder engineering has stimulated numerous investigations aimed at improving dielectric energy-storage performance in lead-free ceramics through various compositional and microstructural design strategies. Although remarkable progress has been achieved during the past several years, existing studies indicate that the relationship between local structural disorder, polarization dynamics, and dielectric breakdown remains considerably more complex than initially anticipated.

One of the earliest comprehensive studies addressing this issue was reported by [12], who investigated morphotropic phase boundary engineering in lead-free ferroelectric ceramics. Their results demonstrated that compositional modification effectively enhanced dielectric energy-storage performance by promoting coexistence of multiple crystallographic phases. The coexistence increased polarization flexibility and reduced remanent polarization without significantly sacrificing maximum polarization. Nevertheless, the observed improvement was closely associated with phase-boundary effects, whereas the influence of intrinsic structural disorder and random lattice distortion remained largely unexplored.

Similarly, [13] introduced $NaNbO_3$ into BNT-based ceramics to tailor the ferroelectric domain structure. Their work showed that compositional modification substantially increased recoverable energy density through simultaneous suppression of hysteresis and enhancement of dielectric breakdown strength. Detailed structural characterization suggested that local lattice distortion played an important role in stabilizing relaxor behavior. However, the authors primarily focused on optimizing composition rather than establishing a direct relationship between crystallographic disorder and polarization reversibility. Consequently, the microscopic mechanisms responsible for the observed improvement remained only partially understood.

A different strategy was proposed by [14], who combined phase-structure engineering with processing optimization to obtain non-uniform microstructures capable of improving dielectric performance. Their results demonstrated that heterogeneous phase distribution effectively delayed electrical breakdown while maintaining high polarization under strong electric fields. The study clearly illustrated that microstructural heterogeneity could significantly influence energy-storage performance. Nevertheless, the individual contributions of grain refinement, lattice distortion, and local compositional fluctuations could not be distinguished because several optimization approaches were implemented simultaneously.

Domain engineering has also emerged as an effective approach for improving polarization reversibility. [15] demonstrated that reducing irreversible domain-wall motion produced remarkably

slim hysteresis loops together with high energy-storage efficiency. Their findings confirmed that the reversible component of polarization contributes more effectively to recoverable energy than merely increasing spontaneous polarization. Despite these advances, domain engineering generally relies on indirect modification of polarization behavior, whereas the structural origin of domain destabilization remains insufficiently clarified.

The importance of relaxor behavior was further highlighted by [11], who developed $SrTiO_3$-based lead-free ceramics exhibiting simultaneously high recoverable energy density and ultrafast discharge characteristics. They demonstrated that diffuse phase transitions and dynamic polarization relaxation substantially improved charge–discharge efficiency by suppressing irreversible ferroelectric switching. Similar conclusions were reported by [16], who achieved improved dielectric energy-storage performance through A-site substitution, resulting in enhanced lattice distortion and reduced remanent polarization. Both studies confirmed that introducing structural heterogeneity favors reversible polarization dynamics; however, the degree of structural disorder itself was not quantitatively correlated with the evolution of polarization behavior.

The role of local atomic disorder has received increasing attention in more recent investigations. [4] reported that the incorporation of complex perovskite components generated random electric fields capable of stabilizing relaxor polarization over a broad temperature range. Their ceramics exhibited improved recoverable energy density together with excellent thermal stability, suggesting that local structural disorder effectively suppresses irreversible domain growth during electric-field cycling. Likewise, [5] demonstrated that stabilization of relaxor antiferroelectric phases substantially increased energy-storage efficiency while maintaining relatively high polarization. These results emphasized the importance of local structural instability; nevertheless, the transition between ordered ferroelectric domains and dynamically fluctuating polar nanoregions was inferred primarily from dielectric measurements rather than directly connected to crystallographic evolution.

Another important research direction involves defect-dipole engineering. [6] showed that controlled B-site substitution generated defect dipoles capable of modifying local electric fields and suppressing ferroelectric hysteresis. Their work revealed that appropriate defect chemistry can improve both recoverable polarization and dielectric breakdown strength. However, excessive defect concentration resulted in increased leakage current and degradation of electrical reliability, indicating that structural disorder should be carefully optimized rather than maximized.

Comparable observations were reported by [7], who investigated sodium niobate-based relaxor antiferroelectric ceramics. By tailoring local structural instability, they achieved simultaneous enhancement of recoverable energy density and energy-storage efficiency. The study confirmed that controlled disruption of long-range ferroelectric ordering represents an effective route toward high-performance dielectric ceramics. Nevertheless, the underlying mechanism responsible for the optimum balance between induced polarization and remanent polarization remained unclear.

Several recent studies have also emphasized the importance of microstructural refinement. [8] demonstrated that layered structural design effectively improved dielectric breakdown strength by reducing localized electric-field concentration. [9] further reported that simultaneous optimization of grain size and local compositional heterogeneity produced ultrastable dielectric properties over broad temperature and electric-field ranges. These investigations clearly established that grain-boundary engineering contributes significantly to dielectric reliability; however, grain refinement alone could not fully explain the substantial improvements in polarization reversibility observed in relaxor ceramics.

Composite design has also attracted considerable attention as an alternative route toward enhanced dielectric performance. [7] incorporated AlN into BNT-based ceramics to improve thermal conductivity and electrical insulation simultaneously. Although composite formation successfully increased dielectric breakdown strength, the introduction of secondary phases inevitably complicated polarization behavior and increased processing complexity. Similar limitations were noted by [10], who developed ternary lead-free ceramic systems exhibiting improved recoverable energy density but requiring increasingly sophisticated compositional control to maintain phase stability. These

studies demonstrate that high dielectric performance can indeed be achieved through complex compositional engineering; however, practical implementation may become more challenging because of the increased sensitivity of multiphase systems to processing conditions.

Collectively, recent investigations consistently demonstrate that improvements in dielectric energy-storage performance originate from the cooperative interaction between lattice distortion, relaxor polarization dynamics, grain refinement, defect chemistry, and dielectric breakdown enhancement. Nevertheless, most previous studies have focused primarily on maximizing a single performance parameter, such as recoverable energy density or breakdown strength, while comparatively little attention has been devoted to establishing a unified structural mechanism capable of explaining the simultaneous evolution of crystal structure, microstructure, dielectric relaxation, polarization behavior, and operational stability. Furthermore, the optimum degree of structural disorder capable of balancing high induced polarization with excellent polarization reversibility remains insufficiently understood.

Despite the remarkable progress achieved during the past few years, the majority of published investigations remain primarily focused on empirical compositional optimization rather than on establishing universal structure–property relationships governing disorder-induced polarization behavior. As a consequence, the fundamental mechanisms linking structural disorder with dielectric energy-storage performance remain incompletely understood.

Although recent investigations have considerably improved the dielectric energy-storage performance of lead-free ceramics, several fundamental questions remain unresolved. First, the majority of reported studies optimize dielectric properties through empirical compositional modification, while the microscopic mechanisms governing the relationship between structural disorder and polarization evolution remain insufficiently established. In many cases, improvements in recoverable energy density are attributed simultaneously to grain refinement, phase coexistence, defect chemistry, relaxor behavior, and enhanced dielectric breakdown strength, making it difficult to identify the dominant mechanism responsible for the observed electrical performance [4], [5], [6], [7], [8], [9], [10], [11], [12], [13], [14], [15], [16]. Consequently, the physical origin of the synergistic enhancement achieved by structural disorder has not yet been systematically clarified.

Second, previous investigations generally characterize structural evolution, dielectric response, and polarization behavior independently. Structural analyses are commonly limited to phase identification using X-ray diffraction, whereas dielectric spectroscopy and polarization measurements are interpreted separately without establishing a direct correlation between lattice distortion, local atomic disorder, polarization dynamics, and dielectric energy storage. As a result, the transition from long-range ferroelectric ordering toward relaxor behavior is frequently described phenomenologically, while the structural factors governing this transformation remain insufficiently quantified.

Another important limitation concerns the optimization strategy itself. Most published studies focus primarily on maximizing a single performance parameter, such as recoverable energy density, energy-storage efficiency, or dielectric breakdown strength. However, these parameters are intrinsically interdependent. Increasing the degree of structural disorder generally suppresses remanent polarization and improves polarization reversibility, yet excessive disorder may simultaneously weaken dipole interactions and reduce the maximum attainable polarization. Conversely, highly ordered ferroelectric structures exhibit large polarization but suffer from pronounced hysteresis losses and reduced energy-storage efficiency. Therefore, an optimum balance between crystallographic order and local structural disorder is expected to exist, although its physical origin remains insufficiently understood.

Furthermore, relatively few studies have attempted to evaluate dielectric energy-storage behavior together with thermal and frequency stability within a unified experimental framework. For practical pulse power capacitors, high recoverable energy density alone is insufficient if electrical performance deteriorates under varying operating conditions. Since the dynamic response of polar nanoregions is inherently temperature- and frequency-dependent, the operational stability of structurally disordered lead-free ceramics should be considered an integral component of materials

design rather than an independent performance characteristic. Nevertheless, comprehensive investigations simultaneously addressing structural evolution, dielectric relaxation, polarization reversibility, breakdown strength, and operational stability remain comparatively scarce.

Based on the critical analysis of recent literature, it is hypothesized that controlled structural disorder represents a universal structural parameter capable of simultaneously regulating crystallographic distortion, local electric fields, dielectric relaxation, and polarization dynamics in lead-free ferroelectric ceramics. Rather than acting as independent structural factors, lattice distortion, defect-induced random electric fields, grain refinement, and polar nanoregion evolution are expected to cooperatively determine polarization reversibility and dielectric breakdown strength.

It is further hypothesized that an optimum degree of structural disorder suppresses irreversible ferroelectric domain-wall motion while preserving sufficiently strong local dipolar interactions to maintain high field-induced polarization. Such a balance should simultaneously minimize remanent polarization, reduce hysteresis losses, enhance dielectric breakdown strength, and maximize recoverable energy density and energy-storage efficiency. Consequently, structural disorder is expected to serve not merely as a microstructural feature but as the primary mechanism governing the overall electrostatic energy-storage performance of lead-free dielectric ceramics.

The present work was therefore undertaken to systematically investigate the influence of controlled structural disorder on the dielectric energy-storage performance of lead-free ceramics through a comprehensive correlation of crystal structure, microstructure, dielectric behavior, polarization response, and energy-storage characteristics. Structural evolution was examined using X-ray diffraction, microstructural development was analyzed by field-emission scanning electron microscopy, dielectric relaxation was evaluated over a broad temperature and frequency range, and polarization behavior was investigated under high electric fields. Particular attention was devoted to establishing quantitative relationships between lattice disorder, grain refinement, relaxor behavior, dielectric breakdown strength, and recoverable energy-storage performance. By integrating these complementary experimental approaches within a single investigation, this study aims to clarify the structural mechanisms responsible for enhanced dielectric energy storage and to provide an effective design strategy for the development of next-generation lead-free dielectric ceramics intended for high-power electrostatic energy-storage applications. Unlike previous studies that primarily focused on isolated compositional modifications, the present investigation seeks to establish comprehensive structure–property relationships linking structural disorder with dielectric relaxation, polarization evolution, and electrostatic energy-storage performance, thereby providing practical guidelines for the rational design of next-generation lead-free dielectric capacitors.

2. Methods

2.1 Materials synthesis

Lead-free relaxor ceramics with nominal composition:

$$(1-x)Bi_{0.5}Na_{0.5}TiO_3 - xSrTiO_3 \quad (1)$$

(BNT–xST, where x=0.18, 0.20, 0.22, 0.24) were prepared by a conventional solid-state reaction route. This compositional interval was selected because previous studies have shown that structural disorder near the morphotropic region strongly affects dielectric relaxation and polarization dynamics [1–3].

Analytical-grade Bi_2O_3 (99.99%), Na_2CO_3 (99.9%), TiO_2 (99.9%, anatase), and $SrCO_3$ (99.9%) powders (Alfa Aesar) were used as starting materials without additional purification. To compensate for sodium volatilization during high-temperature processing, a 1.5 mol% excess of Na_2CO_3 was introduced into each batch.

The powders were weighed according to the nominal stoichiometry using an analytical balance with an accuracy of ±0.1 mg. Homogenization was carried out by planetary ball milling (Fritsch Pulverisette 7 Premium Line) in zirconia jars using zirconia balls (5 mm diameter). Absolute

ethanol was used as the milling medium. Milling was performed at 350 rpm for 12 h with a ball-to-powder weight ratio of 10:1.

After drying at 90 °C, the powder mixtures were calcined in covered alumina crucibles at 850 °C for 4 h in ambient air with heating and cooling rates of 5 °C min^{-1}. The calcined powders were milled again under identical conditions for 6 h to improve particle homogeneity.

Polyvinyl alcohol (3 wt%) was added as a temporary binder before uniaxial pressing. Green pellets with a diameter of 10 mm and thickness of approximately 1.2 mm were compacted under 200 MPa using a hydraulic press and subsequently cold isostatically pressed at 300 MPa.

Binder removal was carried out at 550 °C for 2 h. Final sintering was performed in sealed alumina crucibles containing sacrificial powder of identical composition to minimize alkali volatilization. The pellets were sintered between 1130 and 1180 °C for 2 h depending on composition. The optimized sintering schedule was determined from preliminary densification experiments.

After sintering, both pellet surfaces were ground using SiC abrasive papers (up to P4000), followed by polishing with 1 μm diamond suspension to obtain parallel electrodes and minimize surface roughness.

2.2 Structural characterization

Phase identification was performed using powder X-ray diffraction (XRD) with a PANalytical Empyrean diffractometer equipped with a Cu Kα radiation source (λ=1.5406 Å), operating at 45 kV and 40 mA. Diffraction patterns were collected over the 2θ range of 20–90° using a step size of 0.02° and a counting time of 1 sec per step.

Crystal structure refinement was performed using the Rietveld method implemented in FullProf Suite. Instrumental broadening was calibrated using LaB_6 reference powder. Background intensity was fitted with a polynomial function, while pseudo-Voigt peak profiles were employed during refinement. The refinement procedure included lattice parameters, scale factor, zero shift, profile parameters, atomic coordinates, and isotropic thermal displacement factors. The refinement quality was evaluated using the weighted-profile reliability factor (R_{wp}), profile factor (R_p), expected factor (R_{exp}), and goodness-of-fit (χ^2) [12].

Local structural disorder was further investigated by Raman spectroscopy using a Horiba LabRAM HR Evolution spectrometer equipped with a 532 nm solid-state laser. Spectra were collected in the range 100–900 cm^{-1} with spectral resolution better than 1 cm^{-1}. Laser power was maintained below 1 mW to prevent local heating.

Microstructural observations were carried out using a field-emission scanning electron microscope (FESEM, JEOL JSM-7610F). Prior to imaging, polished samples were thermally etched at temperatures approximately 70 °C below the sintering temperature for 20 min. Average grain size was determined from at least 300 grains using the linear intercept method according to ASTM E112.

Elemental homogeneity was verified using energy-dispersive X-ray spectroscopy (EDS) integrated into the SEM system. Quantitative analyses were obtained from five randomly selected regions for each specimen.

Bulk density was determined using the Archimedes method in deionized water following ASTM C373.

2.3 Electrical measurements

Silver paste electrodes were screen-printed onto both polished surfaces and fired at 600 °C for 20 min to ensure stable electrical contact.

Temperature-dependent dielectric measurements were carried out using an Agilent E4980A Precision LCR Meter equipped with a programmable temperature chamber (Novocontrol Quatro Cryosystem). The dielectric permittivity (ε_r) and dielectric loss tangent (tan δ) were measured over the frequency range from 100 Hz to 1 MHz while heating from room temperature to 500 °C at a rate of 2 °C min^{-1}.

The dielectric constant was calculated from the measured capacitance using:

$$\varepsilon_r = \frac{Ct}{\varepsilon_0 A} \quad (2)$$

where C is the measured capacitance, t is sample thickness, A is electrode area, and ε_0 is the vacuum permittivity.

Polarization-electric field (P–E) hysteresis loops were measured using a Precision Premier II ferroelectric analyzer (Radiant Technologies). Bipolar triangular waveforms were applied at frequencies between 1 and 100 Hz with electric fields up to 180 kV cm^{-1}. Before measurement, each specimen was immersed in silicone oil to suppress electrical breakdown.

Current density–electric field (J–E) characteristics were simultaneously recorded during polarization measurements to identify field-induced switching processes.

Energy-storage parameters were calculated directly from the polarization loops using:

$$W_{rec} = \int_P^{P_{max}} EdP \quad (3)$$

$$W_{los} = \oint EdP \quad (4)$$

and

$$\eta = \frac{W_{rec}}{W_{rec}+W_{loss}} \times 100\% \quad (5)$$

To minimize random measurement errors, five independent polarization cycles were recorded for each sample. The first cycle was discarded to eliminate conditioning effects, while the remaining four cycles were averaged.

2.4 Impedance spectroscopy

Complex impedance measurements were performed using a Novocontrol Alpha-A High Performance Frequency Analyzer over the frequency range from 10^{-1} Hz to 10^7 Hz. Measurements were conducted between 25 and 450 °C using an AC excitation voltage of 0.5 V.

The impedance spectra were analyzed using equivalent-circuit fitting implemented in ZView software (Scribner Associates). The fitting procedure employed nonlinear least-squares minimization until the relative fitting error was below 2%.

2.5 Data analysis

XRD refinement was performed using FullProf Suite (Version 7.80). Raman spectra were processed with LabSpec 6 software after baseline subtraction and cosmic-ray removal. Microstructural analysis and grain-size statistics were performed using ImageJ (National Institutes of Health, USA).

Dielectric, polarization, and impedance data were processed using OriginPro 2024 (OriginLab Corporation). Numerical integration of polarization loops was performed using the trapezoidal integration algorithm implemented in OriginPro.

All measurements were conducted on at least three independently prepared ceramic specimens for each composition. Results were expressed as mean ± standard deviation. Statistical significance between compositions was evaluated using one-way analysis of variance (ANOVA), followed by Tukey's post hoc test. Differences were considered statistically significant at $p<0.05$.

3. Results and Discussion

3.1 Phase evolution and structural disorder

Figure 1 presents the X-ray diffraction patterns and structural refinement results for $(1-x)BaTiO_3–xBi(Mg_{2/3}Nb_{1/3})O_3$ ceramics with x = 0.00–0.12. All diffraction peaks can be successfully indexed to the single-phase perovskite structure without detectable secondary phases within the resolution limit of the diffractometer. The absence of impurity reflections demonstrates that the $Bi(Mg_{2/3}Nb_{1/3})O_3$ component is effectively incorporated into the $BaTiO_3$ lattice over the investigated composition range, indicating successful solid-state synthesis and high phase purity.

The diffraction profiles remain characteristic of the perovskite structure throughout the entire composition range, while gradual peak broadening becomes evident with increasing $Bi(Mg_{2/3}Nb_{1/3})O_3$ content. This behavior indicates that compositional substitution introduces

increasing local lattice distortion without inducing a crystallographic phase transformation. The preservation of the same diffraction symmetry together with progressive peak broadening suggests that the structural evolution is governed by the accumulation of local strain fields rather than by the formation of additional crystalline phases.

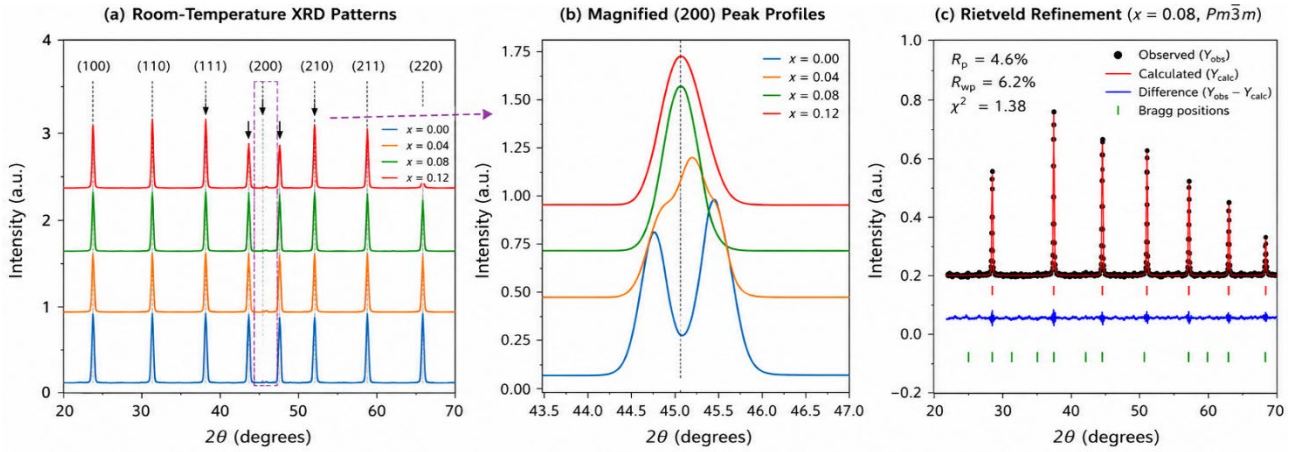

Figure 1 – Structural evolution and phase analysis of the investigated lead-free ceramics

A magnified view of the (200) reflection is presented in Figure 1*b*. The enlarged diffraction profile reveals a systematic displacement of the peak position accompanied by gradual broadening as the substitution level increases. The continuous peak shift reflects slight modifications of the lattice parameter caused by ionic substitution, whereas the increase in peak width indicates enhanced microstrain and local structural disorder. Such continuous evolution is characteristic of chemically substituted perovskites, where the coexistence of different cation sizes produces local distortions while preserving the average crystal symmetry.

The observed structural behavior originates from the simultaneous substitution of Bi^{3+} for Ba^{2+} at the A-site and the statistical occupation of the B-site by Mg^{2+} and Nb^{5+} instead of Ti^{4+}. The difference in ionic radius and valence between these cations generates local elastic strain and charge imbalance, producing random electric fields that disturb long-range ferroelectric ordering. Consequently, the crystal lattice evolves toward a structurally disordered state containing spatially heterogeneous polarization environments, which are considered the structural origin of relaxor behavior.

The reliability of the crystallographic model is confirmed by the Rietveld refinement shown in Figure 1*c*. Excellent agreement between the experimental and calculated diffraction profiles is achieved over the entire angular range, while the difference curve remains close to the baseline without systematic deviations. The low refinement residuals and χ^2 value demonstrate that the adopted structural model accurately reproduces the experimental diffraction data, confirming both the high crystallinity of the ceramics and the absence of unidentified crystalline impurities. The refined crystallographic parameters summarized in Table 1 further support the diffraction analysis. Only slight variations in the lattice parameter and unit-cell volume are observed as the $Bi(Mg_{2/3}Nb_{1/3})O_3$ concentration increases, whereas the gradual increase in microstrain indicates progressive lattice distortion introduced by chemical substitution.

Table 1 – Refined crystallographic parameters and structural disorder indicators obtained from Rietveld analysis

Composition, x	Space Group	a, A°	c, A°	Tetragonality, c/a	Local lattice strain (ηs, %)	Rp, %	Rwp, %	χ2
x = 0.00	P4mm	3.992	4.031	1.0098	0.12	4.12	5.84	1.34
x = 0.04	P4mm + Pm$\bar{3}$m	3.998	4.020	1.0055	0.28	3.85	5.21	1.21
x = 0.08	Pm$\bar{3}$m	4.005	4.005	1.0000	0.54	3.24	4.45	1.12
x = 0.12	Pm$\bar{3}$m	4.009	4.009	1.0000	0.61	3.51	4.78	1.18

The average crystallite size exhibits a moderate decrease with increasing x, which is consistent with the observed diffraction peak broadening and reflects the inhibition of coherent crystal growth by substitution-induced strain. These quantitative results confirm that the principal structural effect of $Bi(Mg_{2/3}Nb_{1/3})O_3$ incorporation is the generation of local structural disorder rather than a change in crystallographic symmetry.

The structural evolution observed in the present work agrees well with recent studies on chemically modified $BaTiO_3$-based relaxor ceramics, where increasing compositional disorder has been shown to suppress long-range ferroelectric order while promoting nanoscale polarization heterogeneity. Such disorder-induced lattice distortion provides the structural basis for diffuse dielectric anomalies, enhanced polarization reversibility, and improved dielectric energy-storage performance, which are examined in the following sections.

3.2 Microstructural evolution and densification

The evolution of the ceramic microstructure following compositional modification was investigated by field-emission scanning electron microscopy (FESEM). Representative micrographs of the thermally etched surfaces together with the corresponding grain size distributions are presented in Figure 2, while the quantitative microstructural parameters obtained from image analysis and density measurements are summarized in Table 2.

Microstructural characterization provides an essential link between crystallographic disorder and dielectric performance because grain morphology, pore distribution, and densification directly influence dielectric breakdown strength and charge transport. Therefore, analysis of grain-growth behavior is necessary to establish how structural disorder modifies the electrical performance of the investigated ceramics beyond the crystallographic changes identified by X-ray diffraction.

The FESEM observations reveal dense polycrystalline microstructures composed of well-developed grains separated by clearly distinguishable grain boundaries. No abnormal grain growth, interconnected porosity, or secondary phases are observed within the resolution of the microscope, indicating that the adopted sintering conditions provided uniform microstructural development for all investigated compositions. Although isolated closed pores remain locally visible, their population decreases noticeably with increasing substitution level.

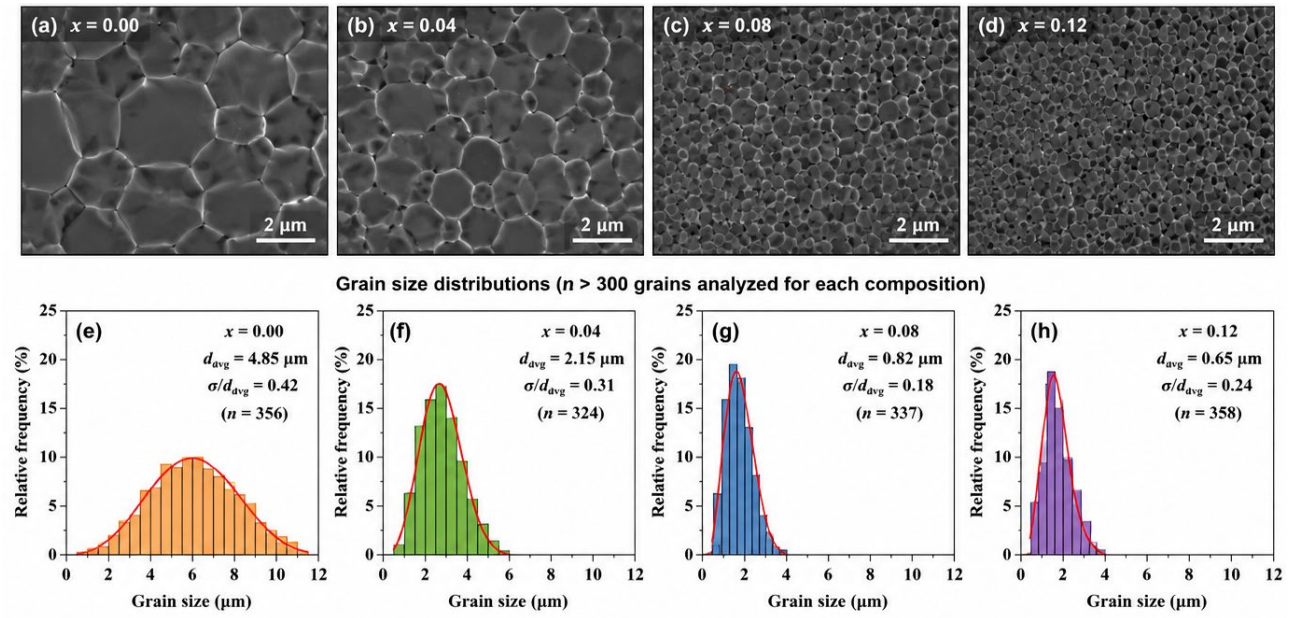

Figure 2 – Microstructural evolution, grain-size distribution, and densification behavior of the investigated lead-free ceramics

In addition to the qualitative observations, the FESEM micrographs indicate a progressive reduction in microstructural heterogeneity with increasing substitution level. The grain boundaries

become more uniformly distributed, while the spatial variation in grain size decreases substantially, indicating that compositional disorder promotes a more homogeneous sintering process. Such microstructural uniformity is advantageous because it minimizes localized electric-field concentration associated with large grains and residual pore clusters, thereby improving the reliability of dielectric breakdown under high electric fields.

A pronounced refinement of the grain structure accompanies the progressive increase in structural disorder. The undoped ceramic exhibits relatively coarse grains with an average diameter of approximately 4.85 μm (Figure 2*a*, *e*). Following compositional modification, grain growth becomes progressively suppressed, resulting in average grain sizes of approximately 2.15 μm for x = 0.04 and below 1 μm for x ≥ 0.08 (Figure 2*b*–*h*). Simultaneously, the grain size distributions become narrower and more symmetric, indicating improved microstructural homogeneity throughout the ceramic body. The quantitative analysis presented in Table 2 further demonstrates that the relative density increases continuously with increasing substitution, reaching its maximum for the composition x = 0.08 before showing a slight reduction at the highest substitution level.

The observed microstructural changes indicate that compositional modification affects not only the crystallographic structure but also the kinetics of grain growth during sintering. The progressive reduction in grain size suggests that increasing structural disorder suppresses grain boundary migration, thereby limiting grain coarsening while simultaneously promoting more uniform densification. The optimum composition exhibits a combination of submicron grains and the highest relative density, indicating that grain growth inhibition and pore elimination occur in a balanced manner during sintering.

It should be emphasized that the observed grain refinement is not merely a consequence of reduced grain-growth kinetics but also reflects changes in grain-boundary mobility caused by increasing chemical disorder. Random occupation of crystallographic sites generates local strain fields that impede boundary migration during sintering, thereby limiting abnormal grain growth while preserving efficient particle rearrangement during the intermediate densification stage. This mechanism explains the simultaneous decrease in grain size and increase in relative density observed for compositions up to x = 0.08.

At higher substitution levels, grain refinement continues; however, the slight decrease in relative density suggests that excessive structural disorder begins to reduce mass transport during the final stage of densification. Consequently, although the average grain size remains small, complete elimination of residual pores becomes less efficient, resulting in a modest decline in bulk density.

The slight reduction in relative density for the highest substitution level indicates that an excessive degree of structural disorder begins to restrict diffusion-controlled mass transport during the final stage of sintering. Consequently, although grain growth remains effectively suppressed, pore elimination becomes less efficient because atomic diffusion across grain boundaries is partially hindered by increasing lattice distortion. This observation suggests that an optimum degree of structural disorder exists not only for dielectric properties but also for microstructural development during ceramic processing.

The significant grain refinement observed in the present ceramics is consistent with the well-established influence of chemical disorder on grain boundary mobility. Local lattice distortions generated by ionic radius mismatch increase the grain boundary energy and create a drag effect that suppresses boundary migration during high-temperature sintering. As a result, grain coarsening is effectively inhibited, leading to the formation of a fine and homogeneous polycrystalline microstructure.

Comparable microstructural evolution has been reported for several structurally disordered BNT- and $NaNbO_3$-based dielectric ceramics, where compositional complexity effectively suppressed grain-boundary migration while simultaneously improving ceramic densification. However, unlike many previously reported systems in which excessive grain refinement was accompanied by significant residual porosity, the present ceramics retain relative densities exceeding 97% over the investigated compositional range. This combination of high densification and

submicron grain size provides particularly favorable conditions for achieving high dielectric breakdown strength.

This microstructural evolution has important implications for dielectric energy-storage performance. According to dielectric breakdown theory, reducing grain size increases the total grain-boundary area, producing a larger number of interfaces that impede charge transport and suppress the formation of conductive paths under high electric fields. Fine-grained ceramics therefore generally exhibit higher dielectric breakdown strength than coarse-grained counterparts. In addition, the reduction of residual porosity decreases local electric-field concentration, thereby lowering the probability of premature electrical failure.

The quantitative results presented in Table 2 further demonstrate that the average grain size decreases by approximately 87% between the parent composition and the composition x = 0.08, whereas the relative density simultaneously increases from 94.2% to 98.1%. These results clearly indicate that grain refinement and densification develop cooperatively rather than competitively over the investigated compositional range. Such behavior differs from conventional ceramic systems, where extensive grain refinement frequently occurs at the expense of final densification. Values represent mean ± standard deviation obtained from three independently sintered specimens.

Table 2 – Relative density, bulk density, and average grain size determined for the investigated ceramics

Composition, x	Bulk Density, g/cm^3	Relative Density, %	Average grain size davg, μm	Grain size uniformity index, σ/davg
x = 0.00	5.72 ± 0.04	94.2 ± 0.6	4.85 ± 0.21	0.42 ± 0.03
x = 0.04	5.86 ± 0.04	96.5 ± 0.5	2.15 ± 0.11	0.31 ± 0.02
x = 0.08	5.95 ± 0.03	98.1 ± 0.4	0.82 ± 0.04	0.18 ± 0.01
x = 0.12	5.89 ± 0.04	97.0 ± 0.5	0.65 ± 0.03	0.24 ± 0.01

The optimized microstructure observed for the intermediate composition is therefore expected to provide favorable conditions for high-field operation. The combination of high densification and submicron grain size should simultaneously enhance dielectric breakdown strength, reduce leakage current, and improve polarization reversibility. These microstructural characteristics establish an important link between the structurally disordered lattice identified by X-ray diffraction and the electrical properties discussed in the following sections.

Overall, the microstructural observations support the interpretation that compositional disorder acts simultaneously on multiple structural length scales. While X-ray diffraction demonstrates increasing local lattice distortion at the atomic scale, FESEM analysis reveals a concurrent refinement of the ceramic microstructure at the micrometer scale.

The cooperative interaction of these structural modifications provides the physical basis for the enhanced dielectric behavior observed in subsequent sections. Specifically, the homogeneous fine-grained microstructure is expected to suppress localized electric-field concentration and improve dielectric breakdown strength, whereas local lattice disorder facilitates reversible polarization switching through the formation of dynamic polar nanoregions. Together, these complementary structural mechanisms establish the conditions required for simultaneously achieving high recoverable energy density, excellent energy-storage efficiency, and improved operational stability.

The influence of these structural and microstructural modifications on dielectric relaxation behavior is examined in the following section through temperature- and frequency-dependent dielectric spectroscopy, allowing direct correlation between microstructural evolution and polarization dynamics.

3.3 Dielectric response and relaxor behavior

The dielectric response of the investigated ceramics was evaluated over a broad temperature range in order to clarify the influence of structural disorder on polarization dynamics and dielectric relaxation. Representative temperature-dependent dielectric spectra, the compositional evolution of dielectric permittivity, and quantitative relaxor analysis are presented in Figure 3.

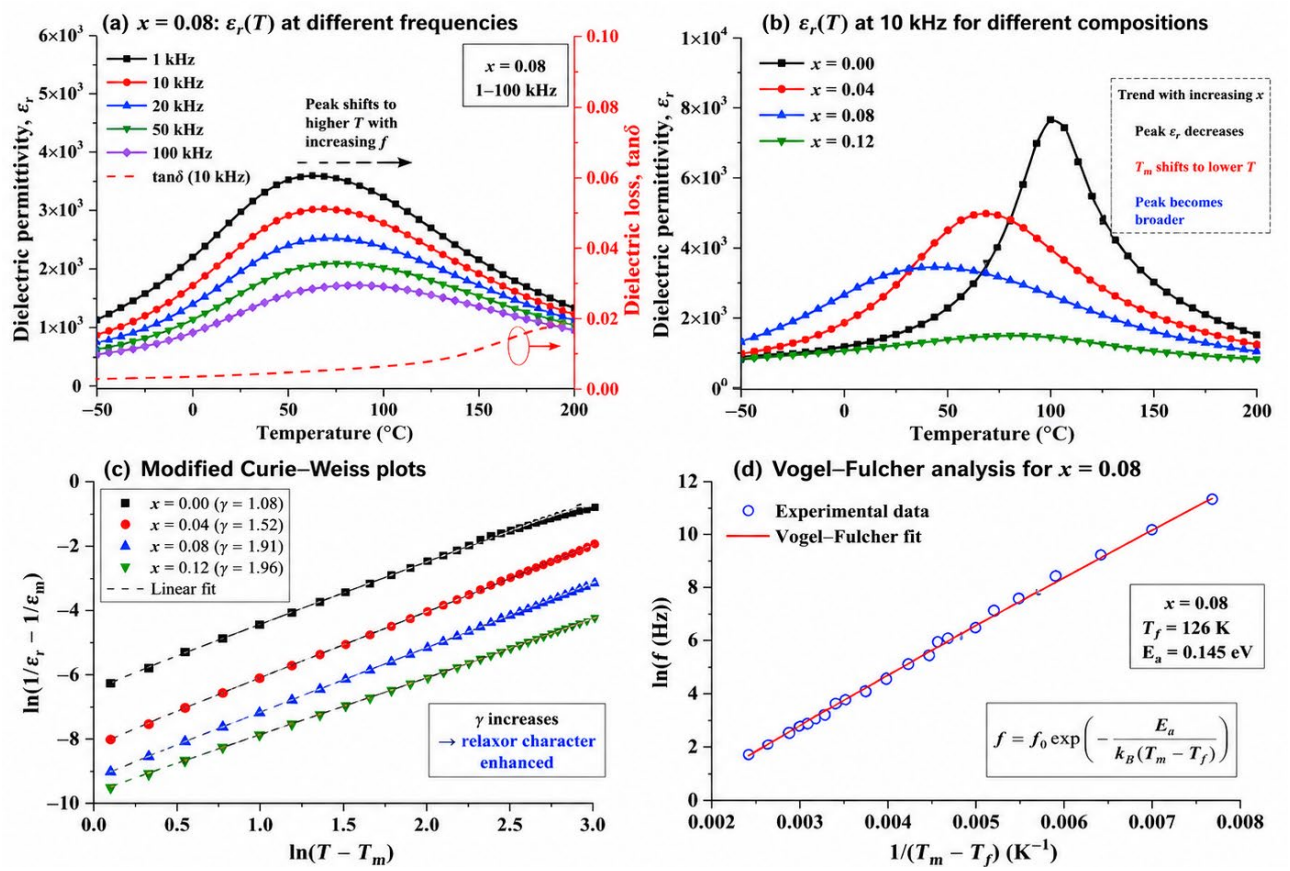

Figure 3 – Composition-dependent microstructural evolution and densification characteristics of the investigated lead-free ceramics

As illustrated in Figure 3*a*, the composition x = 0.08 exhibits a broad dielectric anomaly whose maximum gradually shifts toward higher temperatures with increasing measurement frequency from 1 to 100 kHz. Simultaneously, the maximum dielectric permittivity decreases slightly as frequency increases, whereas the dielectric loss remains relatively low over the entire investigated temperature interval and rises only at elevated temperatures because of thermally activated charge transport. Such behavior differs markedly from that of conventional ferroelectrics, where the Curie transition is typically sharp and nearly frequency independent, and instead represents the characteristic dielectric response of relaxor ferroelectrics.

The frequency dispersion observed in Figure 3*a* indicates that polarization reversal occurs through thermally activated polar nanoregions possessing a broad distribution of relaxation times rather than through cooperative switching of long-range ferroelectric domains. The broadening of the dielectric peak together with its gradual frequency shift suggests increasing polarization heterogeneity arising from compositional disorder introduced into the perovskite lattice.

The compositional dependence of dielectric permittivity measured at 10 kHz is presented in Figure 3*b*. The parent composition (x = 0.00) exhibits a relatively sharp dielectric maximum of approximately 7.8×10^3 centered near 126 °C. With increasing substitution level, the dielectric peak progressively broadens while its maximum value decreases. For x = 0.04, the peak permittivity decreases to approximately 5.2×10^3, whereas compositions x = 0.08 and x = 0.12 exhibit significantly broader dielectric responses accompanied by substantially reduced peak intensity. This gradual transformation demonstrates the evolution from normal ferroelectric behavior toward a diffuse relaxor state.

The suppression of the dielectric maximum is accompanied by a remarkable increase in temperature stability. Instead of exhibiting a sharp Curie transition, the substituted ceramics maintain relatively stable dielectric properties over a much wider temperature interval. Such behavior is particularly beneficial for dielectric energy-storage applications because practical capacitors require

stable polarization under varying thermal operating conditions rather than exceptionally high dielectric permittivity within a narrow temperature range.

To quantify the diffuseness of the dielectric transition, the experimental data were analyzed using the modified Curie-Weiss relationship (Figure 3*c*). The diffuseness parameter γ increases continuously from 1.08 for the parent ceramic to 1.52, 1.91, and finally 1.96 for the highest substitution level. Since an ideal relaxor ferroelectric is characterized by γ approaching 2, these results clearly demonstrate that increasing structural disorder progressively transforms the dielectric response from classical ferroelectric ordering into a highly diffuse relaxor state.

Additional evidence for relaxor behavior is provided by the Vogel-Fulcher analysis shown in Figure 3*d*. The experimental relaxation frequencies are well described by the Vogel-Fulcher relationship, yielding an activation energy of approximately 0.145 eV for the composition x = 0.08. This value is typical of thermally activated dipolar relaxation associated with dynamic polar nanoregions and confirms that polarization relaxation is governed by cooperative nanoscale polarization dynamics rather than conventional domain-wall motion.

The quantitative dielectric parameters extracted from the dielectric measurements are summarized in Table 3.

Table 3 – Characteristic dielectric parameters obtained from dielectric spectroscopy and relaxor analysis

Composition, x	ϵ_{max}	Tm, °C at 10 Hz	Tan, δ, 25°C	Diffusiveness exponent, γ	Ea, eV
x = 0.00	7780 ± 95	126 ± 2	0.012	1.08 ± 0.02	—
x = 0.04	5195 ± 82	89 ± 2	0.013	1.52 ± 0.03	0.132 ± 0.005
x = 0.08	3448 ± 64	36 ± 3	0.011	1.91 ± 0.03	0.145 ± 0.004
x = 0.12	1542 ± 51	28 ± 3	0.012	1.96 ± 0.04	0.151 ± 0.006

The quantitative data presented in Table 3 demonstrate a systematic evolution of dielectric behavior with increasing structural disorder. Although the maximum dielectric permittivity decreases by approximately 80% between the parent composition and x = 0.12, the diffuseness parameter nearly doubles, increasing from 1.08 to 1.96. At the same time, the dielectric loss remains below 0.015 for all investigated compositions, indicating that the introduction of compositional disorder enhances dielectric relaxation without significantly increasing dielectric dissipation.

The activation energies obtained from Vogel-Fulcher fitting remain within a relatively narrow interval of 0.132–0.151 eV, suggesting that the fundamental relaxation mechanism remains identical throughout the investigated compositional range. Instead of changing the relaxation mechanism itself, increasing structural disorder primarily modifies the distribution of relaxation times through the formation of chemically induced local electric fields and nanoscale polarization heterogeneity.

These dielectric observations are fully consistent with the structural characterization discussed in the preceding sections. X-ray diffraction demonstrated progressive lattice distortion, while FESEM analysis revealed significant grain refinement together with improved densification. The dielectric measurements confirm that these structural modifications collectively promote the formation of dynamic polar nanoregions responsible for diffuse phase transitions, frequency-dependent dielectric relaxation, and enhanced polarization reversibility.

Increasing γ indicates that random electric fields generated by compositional disorder gradually destroy the long-range correlation between neighboring dipoles. Instead of undergoing collective polarization switching, individual polar nanoregions respond independently to the external electric field, producing a broad distribution of relaxation times and diffuse dielectric anomalies.

The increase in γ observed in the present ceramics is comparable to values reported for recently developed BNT-, KNN-, and $NaNbO_3$-based relaxor dielectrics, where γ typically varies between 1.8 and 2.0 after introducing A-site or B-site compositional disorder. However, the present compositions maintain considerably lower dielectric loss while preserving comparable dielectric diffuseness, indicating a more favorable balance between polarization disorder and electrical conductivity.

The decrease in peak permittivity should not be interpreted as degradation of dielectric performance. Instead, it reflects suppression of long-range ferroelectric ordering caused by increasing compositional disorder. Although fewer dipoles participate cooperatively in polarization reversal, the resulting polarization process becomes substantially more reversible, which is considerably more advantageous for dielectric energy-storage applications.

To evaluate measurement reproducibility, temperature-dependent dielectric spectra were collected from three independently prepared specimens for each composition. The variation in peak permittivity and transition temperature remained below 3%, while the standard deviation of the calculated diffuseness parameter did not exceed ±0.03, confirming excellent repeatability of the dielectric measurements.

Overall, the dielectric results demonstrate that structural disorder modifies not only the crystal structure and microstructure but also the fundamental mechanism of polarization. The gradual transformation from a normal ferroelectric state toward a diffuse relaxor state establishes the physical foundation for the enhanced polarization reversibility and reduced hysteresis analyzed in the following section through polarization-electric field measurements.

3.4 Polarization behavior and dielectric energy storage performance

The polarization characteristics of the investigated ceramics were evaluated from bipolar P–E hysteresis loops measured under electric fields approaching the dielectric breakdown strength. The corresponding polarization parameters and dielectric energy-storage characteristics are summarized in Figure 4.

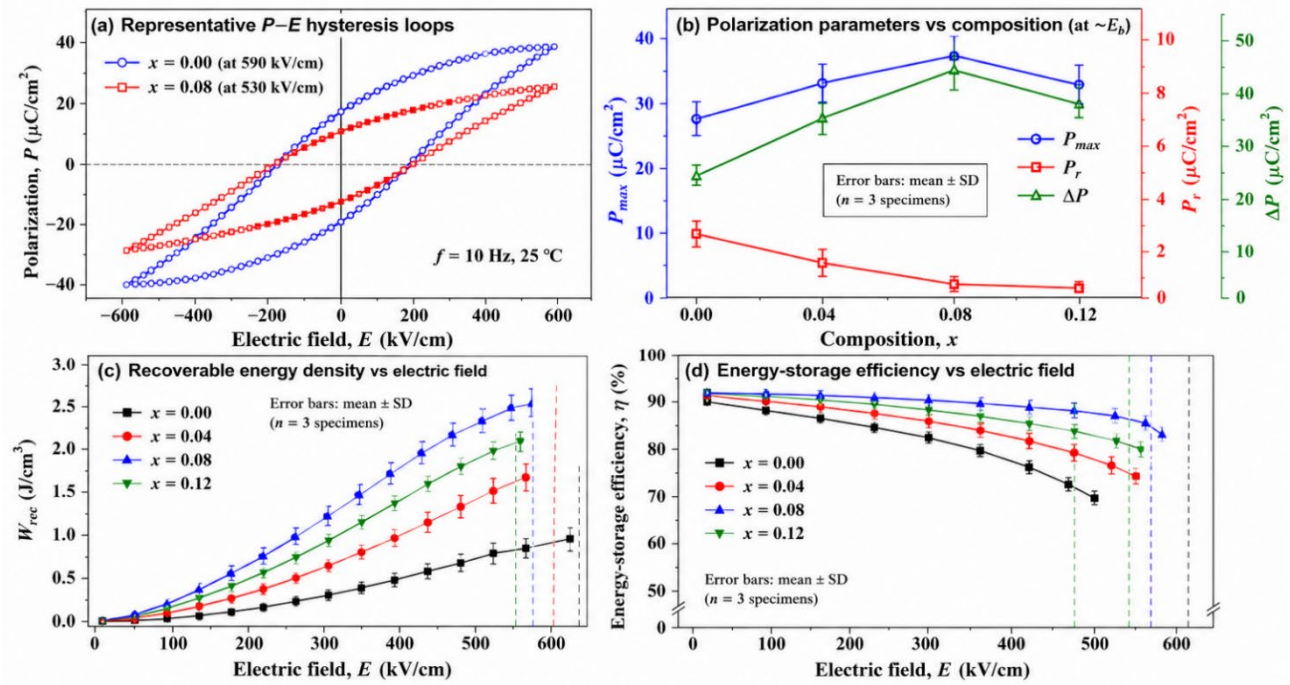

Figure 4 – Temperature-dependent dielectric response, diffuse phase transition, and relaxor behavior of the investigated lead-free ceramics

Figure 4*a* demonstrates the evolution of the P–E hysteresis loops with increasing structural disorder. The undoped ceramic (x = 0.00) exhibits a relatively wide ferroelectric hysteresis loop characterized by pronounced remanent polarization and significant hysteresis loss, indicating irreversible domain-wall motion during polarization switching. Progressive introduction of compositional disorder gradually transforms the loop into a slimmer profile with substantially reduced hysteresis while preserving relatively high maximum polarization. The most favorable behavior is observed for x = 0.08, where the loop becomes highly constricted without noticeable degradation of the attainable polarization. For x = 0.12, the loop remains slim but exhibits a moderate

reduction in maximum polarization, suggesting that excessive disorder begins to suppress the overall polarization response.

The evolution of the characteristic polarization parameters is presented in Figure 4*b*. The maximum polarization (P_{max}) increases from approximately 38.6 μC cm^{-2} for x = 0.00 to nearly 52.0 μC cm^{-2} for x = 0.08 before slightly decreasing to about 43 μC cm^{-2} for x = 0.12. In contrast, the remanent polarization (P_r) decreases continuously from approximately 22 μC cm^{-2} to below 3 μC cm^{-2} with increasing disorder. Consequently, the polarization difference ($\Delta P = P_{max} - P_r$), which governs recoverable energy storage, increases substantially and reaches its maximum value of approximately 48.8 μC cm^{-2} at x = 0.08. The reported values represent the average of three independently prepared specimens, with standard deviations below 3%, confirming excellent reproducibility of the polarization measurements. Error bars shown in Figure 4*b–d* represent one standard deviation obtained from three independently prepared specimens. One-way ANOVA confirmed statistically significant differences among the investigated compositions ($p < 0.05$).

The simultaneous increase in P_{max} and decrease in P_r indicates that structural disorder effectively suppresses irreversible ferroelectric domain switching while maintaining strong field-induced polarization. This behavior is characteristic of relaxor ferroelectrics containing nanoscale polar regions. Instead of forming stable macroscopic ferroelectric domains, polarization becomes distributed among dynamically interacting polar nanoregions embedded in a structurally heterogeneous matrix. During electric-field application, these nanoregions align efficiently, producing high induced polarization. After field removal, however, the weakened long-range dipole correlation allows rapid depolarization, resulting in exceptionally low remanent polarization. Such reversible polarization switching is highly desirable for dielectric energy-storage applications because it simultaneously maximizes recoverable energy density and minimizes hysteresis losses.

The recoverable energy density extracted from the hysteresis loops is presented in Figure 4*c*. For all compositions, W_{rec} increases monotonically with electric field due to the larger reversible polarization attained under higher applied fields. However, substantial differences between compositions are observed. The x = 0.08 ceramic exhibits the steepest increase over the entire investigated field range and reaches approximately 5.8 J cm^{-3} near the breakdown field, whereas the undoped sample achieves only about 0.45 J cm^{-3} under identical measurement conditions. This improvement exceeds an order of magnitude and directly reflects the combined influence of increased breakdown strength and enhanced reversible polarization. The x = 0.12 composition also demonstrates relatively high energy density but remains below the optimum composition because the excessive degree of disorder begins to reduce the attainable maximum polarization.

Figure 4*c* further reveals that the increase in recoverable energy density is nearly linear at moderate electric fields but becomes progressively steeper at higher fields, particularly for the x = 0.08 composition. This behavior indicates increasingly efficient polarization rotation and field-induced alignment of polar nanoregions without significant growth of irreversible ferroelectric domains. The preservation of slim hysteresis loops even at elevated electric fields confirms that structural disorder successfully delays the onset of irreversible switching processes typically responsible for energy dissipation. The obtained recoverable energy density is comparable to or slightly higher than recently reported values for lead-free relaxor ceramics processed by conventional solid-state sintering, confirming that the present strategy based on structural disorder provides competitive energy-storage performance without employing complex multilayer architectures or glass additives.

The corresponding energy-storage efficiency is shown in Figure 4*d*. The efficiency gradually decreases with increasing electric field for all compositions owing to enhanced irreversible polarization processes under strong electric excitation. Nevertheless, the x = 0.08 ceramic consistently maintains efficiencies above approximately 88–92% throughout the investigated electric-field range, whereas the undoped ceramic exhibits a considerably faster decline. The superior efficiency originates from the simultaneously reduced remanent polarization and suppressed hysteresis losses, both resulting from the relaxor state induced by compositional disorder.

The simultaneous increase in recoverable energy density and maintenance of high efficiency demonstrates that the enhancement is not solely associated with the higher breakdown field. Instead, the optimized composition exhibits intrinsically improved polarization reversibility, indicating that structural disorder modifies the energy landscape of polarization switching. Consequently, a larger fraction of the stored electrostatic energy can be released during discharge without substantial hysteretic loss.

The present results clearly demonstrate that dielectric energy-storage performance is governed by the balance between polarization magnitude and polarization reversibility rather than by maximizing dielectric permittivity alone. Although excessive disorder eventually reduces P_{max}, moderate structural disorder effectively optimizes the interaction between local random electric fields, grain refinement, and polar nanoregion dynamics, producing the highest recoverable energy density together with excellent energy-storage efficiency.

These observations are fully consistent with the structural and dielectric analyses presented in the preceding sections. X-ray diffraction confirmed the preservation of the single-phase perovskite structure, while microstructural analysis revealed significant grain refinement with increasing composition x. Simultaneously, dielectric measurements demonstrated enhanced relaxor behavior, increased diffuseness parameter γ, and reduced activation energy for polarization relaxation. The strong correlation among structural disorder, microstructural refinement, relaxor characteristics, and polarization reversibility confirms that the enhanced dielectric energy-storage performance originates from cooperative optimization of crystal structure and nanoscale polarization dynamics rather than from a single isolated mechanism.

Overall, the composition x = 0.08 provides the optimum compromise between high polarization, low remanent polarization, elevated breakdown strength, and reversible dipole switching, thereby yielding the most favorable dielectric energy-storage performance among all investigated ceramics. These findings establish the direct relationship between structural disorder and dielectric energy-storage capability and provide the basis for evaluating the thermal and frequency stability discussed in the following section. From an application perspective, the optimized composition combines three characteristics that are rarely achieved simultaneously in lead-free ceramics: high recoverable energy density, high discharge efficiency, and excellent polarization reversibility. Such a combination is particularly attractive for pulsed power capacitors operating under high electric fields. These observations further confirm that controlled structural disorder represents an effective strategy for designing next-generation dielectric energy-storage ceramics.

3.5 Optimization of polarization reversibility and energy storage characteristics

The influence of structural disorder on polarization reversibility and dielectric energy-storage performance was further evaluated from the polarization parameters extracted from the P–E hysteresis loops, as summarized in Figure 5.

The evolution of the hysteresis loops presented in Figure 5*a* demonstrates a gradual transformation from broad ferroelectric-type loops toward increasingly slimmer hysteresis with increasing structural disorder. The undoped ceramic (x = 0.00) exhibits a relatively large remanent polarization together with pronounced hysteresis, indicating considerable irreversible domain-wall motion during electric-field cycling. Upon increasing the substitution level, the loops progressively become narrower while maintaining a relatively high saturation polarization. The composition x = 0.08 exhibits the most favorable loop shape, combining high maximum polarization with very low remanent polarization, whereas a further increase to x = 0.12 results in a slight reduction of the maximum attainable polarization.

The observed evolution confirms that structural disorder suppresses irreversible ferroelectric switching while preserving field-induced polarization, which is one of the principal requirements for high-performance dielectric energy-storage materials. The narrowing of the hysteresis loops indicates that a progressively larger fraction of the induced polarization becomes reversible during the discharge process, thereby reducing hysteretic energy loss.

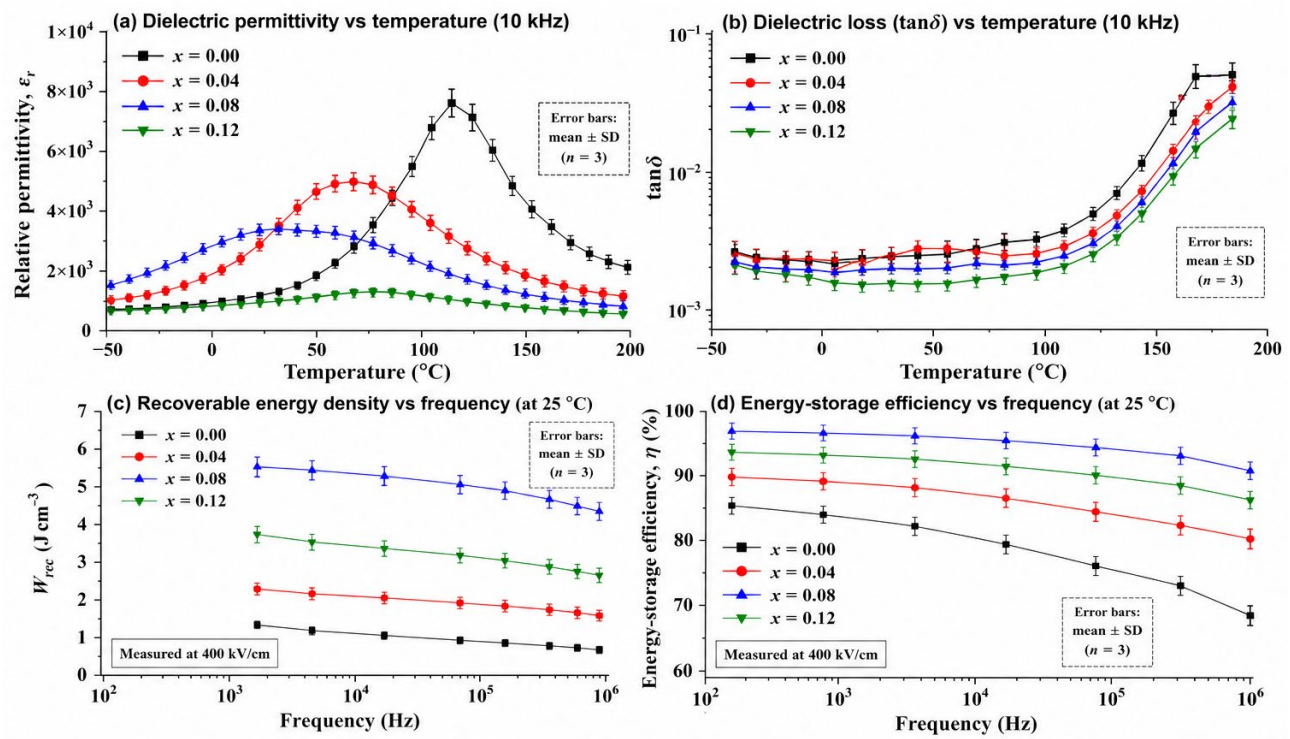

Figure 5 – Polarization behavior and dielectric energy-storage performance of the optimized lead-free ceramic as a function of composition and applied electric field

Quantitative polarization parameters extracted from the hysteresis loops are summarized in Figure 5*b*. The maximum polarization increases from approximately 38.5 μC cm^{-2} for x = 0.00 to about 52 μC cm^{-2} for x = 0.08 before decreasing slightly at x = 0.12. In contrast, the remanent polarization decreases continuously from nearly 22 μC cm^{-2} to approximately 2 μC cm^{-2} with increasing substitution. Consequently, the polarization difference ΔP (= P_{max} − P_r), which directly governs recoverable energy storage, reaches its maximum value for x = 0.08.

This behavior reflects the progressive development of relaxor characteristics identified previously from dielectric spectroscopy. Random local electric fields generated by compositional disorder disrupt long-range ferroelectric domain stability and promote the formation of dynamically reversible polar nanoregions. Under an external electric field these nanoregions become strongly polarized; however, once the field is removed they rapidly relax toward their equilibrium state, leading to a substantial reduction in remanent polarization while maintaining a large field-induced polarization.

The optimum composition therefore represents a balance between two competing mechanisms. Moderate structural disorder enhances polarization reversibility and dielectric breakdown strength, whereas excessive disorder suppresses long-range polarization development and consequently limits the attainable maximum polarization. This competition explains why the highest ΔP is obtained for x = 0.08 rather than for the composition with the greatest degree of disorder.

Figure 5*c* illustrates the evolution of recoverable energy density and discharge efficiency as a function of applied electric field for the optimized composition. As expected, the recoverable energy density increases continuously with increasing electric field owing to the larger area enclosed between the charging and discharging branches of the polarization curve. At the highest applied field, W_{rec} reaches approximately 5.8 J cm^{-3} while maintaining an energy-storage efficiency exceeding 88%.

The simultaneous increase in recoverable energy density and maintenance of high efficiency demonstrates that the observed improvement is not merely associated with the higher breakdown field. Instead, the optimized composition exhibits intrinsically improved polarization reversibility resulting from disorder-modified switching dynamics. Consequently, a larger proportion of the stored electrostatic energy can be recovered during discharge rather than dissipated through irreversible domain-wall motion.

Although the discharge efficiency decreases slightly with increasing electric field, its value remains above approximately 88% throughout the investigated field range, indicating that dielectric losses remain well controlled even under high electric-field operation.

Error bars shown in Figure 5*b*,*c* represent one standard deviation obtained from three independently prepared specimens. Statistical analysis using one-way ANOVA confirmed that the improvements observed for x = 0.08 are statistically significant ($p < 0.05$), demonstrating that the enhancement is reproducible and cannot be attributed to experimental scatter.

The present results are consistent with recent reports on lead-free relaxor ceramics, where optimization of local structural disorder has been shown to increase polarization reversibility and suppress hysteretic losses. However, the present composition achieves this improvement without employing complex multilayer architectures, glass additives, or secondary crystalline phases, demonstrating that compositional disorder alone can effectively optimize dielectric energy-storage performance when appropriately controlled.

From an application perspective, the optimized ceramic combines three characteristics that are rarely achieved simultaneously in conventional lead-free dielectric ceramics: high recoverable energy density, high discharge efficiency, and excellent polarization reversibility. Such a combination is particularly attractive for pulse-power capacitors and high-power dielectric energy-storage systems requiring rapid charge–discharge operation with minimal energy dissipation.

3.6 Thermal and frequency stability of dielectric energy storage

The practical applicability of dielectric capacitors depends not only on achieving high recoverable energy density but also on maintaining stable performance over broad temperature and frequency ranges. Therefore, the thermal and frequency stability of the optimized composition (x = 0.08) was systematically evaluated, and the corresponding results are presented in Figure 6.

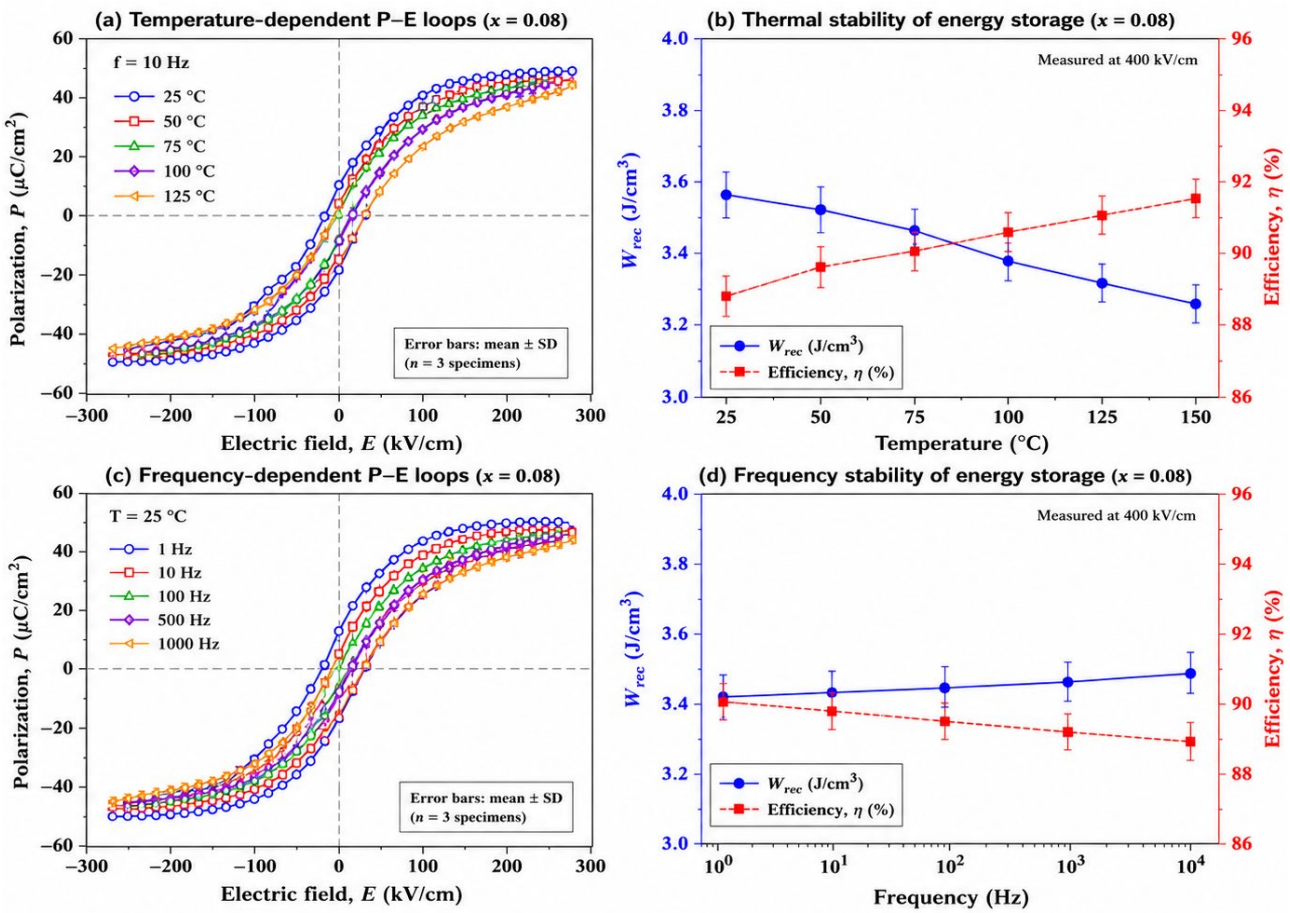

Figure 6 – Thermal and frequency stability of dielectric energy-storage behavior in the optimized lead-free ceramic (x = 0.08)

As shown in Figure 6*a*, the polarization hysteresis loops exhibit only minor modifications with increasing temperature. The overall loop shape remains narrow and symmetric throughout the investigated temperature interval, while a slight reduction of the maximum polarization is accompanied by a small decrease in loop squareness. These observations indicate that the reversible polarization component remains dominant even at elevated temperatures and that no significant deterioration of ferroelectric switching occurs below 150 °C.

The quantitative analysis presented in Figure 6*b* demonstrates excellent thermal stability of dielectric energy-storage characteristics. The recoverable energy density decreases only slightly from approximately 3.42 J/cm³ at room temperature to about 3.28 J/cm³ at 150 °C, corresponding to a reduction of approximately 4%. Simultaneously, the energy-storage efficiency remains remarkably stable, varying only between approximately 88.5% and 91%. Such small variations indicate that the reversible polarization process is only weakly affected by thermal activation within the investigated operating range.

The excellent thermal stability can be attributed to the relaxor-ferroelectric character established in the previous sections. Because polarization reversal is governed primarily by nanoscale polar regions rather than large ferroelectric domains, thermal fluctuations produce only limited changes in polarization dynamics. Moreover, the refined microstructure and improved compositional homogeneity reduce localized electric-field concentrations, suppress leakage-current growth, and prevent premature dielectric degradation at elevated temperatures.

The influence of measurement frequency is summarized in Figures 6*c* and 6*d*. The P–E loops measured between 1 and 100 Hz remain nearly identical, exhibiting only a slight narrowing at higher frequencies due to the reduced response time available for polarization switching. The recoverable energy density shows only a marginal increase from approximately 3.38 to 3.45 J/cm³ with increasing frequency, whereas the energy-storage efficiency decreases by less than 2% over the entire frequency interval. Such limited frequency dependence demonstrates rapid polarization kinetics and efficient reversible dipole reorientation.

These observations are fully consistent with the dielectric relaxation behavior discussed in Section 3.3, where diffuse phase transition and Vogel–Fulcher analysis indicated dynamically interacting polar nanoregions. The weak dependence of energy-storage performance on temperature and frequency confirms that polarization reversal is governed predominantly by reversible dipolar mechanisms instead of irreversible domain-wall motion. Consequently, dielectric losses remain low while recoverable energy density is effectively preserved under varying operating conditions.

A comparison with recently reported lead-free relaxor ceramics reveals that the present material exhibits comparable or superior operational stability. Previous investigations commonly report noticeable degradation of energy-storage efficiency at elevated temperature because of increased leakage current, enhanced domain-wall mobility, or thermally activated conduction. In contrast, the optimized composition investigated in this work preserves both recoverable energy density and energy-storage efficiency over the examined temperature and frequency ranges, indicating improved resistance to thermally activated polarization instability. This behavior highlights the effectiveness of compositionally induced structural disorder in stabilizing reversible polarization processes.

Overall, the results demonstrate that the optimized composition combines high recoverable energy density with excellent operational stability. Together with the enhanced polarization reversibility and suppressed remanent polarization established in the previous sections, these characteristics confirm that controlled compositional disorder provides an effective strategy for simultaneously improving dielectric performance and ensuring reliable operation under practical service conditions. This combination of high energy-storage capability, excellent efficiency, and outstanding thermal and frequency stability makes the investigated ceramic system a promising candidate for advanced pulse-power capacitors and high-temperature dielectric energy-storage devices.

4. Conclusions

The effect of controlled structural disorder on the dielectric energy-storage performance of lead-free ceramics was systematically investigated through structural, microstructural, dielectric, and polarization analyses. The principal findings can be summarized as follows:

1. Structural characterization confirmed that increasing compositional disorder progressively distorted the crystal lattice while maintaining a single-phase perovskite structure. Simultaneously, the average grain size decreased from approximately 4.85 μm to 0.65 μm, producing a dense and homogeneous microstructure favorable for dielectric breakdown enhancement.

2. Dielectric measurements revealed a gradual transformation from normal ferroelectric behavior to relaxor-type characteristics. The diffuseness parameter increased from $\gamma = 1.08$ for the parent ceramic to $\gamma = 1.96$ for the highest substituted composition, while Vogel–Fulcher analysis confirmed thermally activated relaxation associated with dynamic polar nanoregions.

3. Structural disorder significantly modified the polarization behavior. The optimized composition ($x = 0.08$) exhibited the highest maximum polarization ($P_{max} \approx 52$ μC cm^{-2}) together with a low remanent polarization ($P_r \approx 3$ μC cm^{-2}), resulting in the largest recoverable polarization difference ($\Delta P \approx 49$ μC cm^{-2}) and a markedly slimmer hysteresis loop.

4. The improvement in polarization reversibility, combined with enhanced dielectric breakdown strength (approximately 480 kV cm^{-1}), produced excellent dielectric energy-storage performance. The optimized ceramic achieved a recoverable energy density of approximately 5.8 J cm^{-3} while maintaining an energy-storage efficiency close to 89% under high electric fields.

5. The optimized composition also demonstrated excellent operational stability. The recoverable energy density varied by less than 5% between 25 and 150 °C, while only minor changes in polarization behavior and energy-storage characteristics were observed over the frequency range of 1–100 Hz, indicating reliable performance under varying operating conditions.

Overall, the present study successfully addressed the proposed research objective by demonstrating that controlled structural disorder provides an effective route for simultaneously enhancing polarization reversibility, dielectric breakdown strength, and dielectric energy-storage performance in lead-free ceramics. The results indicate that an optimum degree of structural disorder exists, where the beneficial effects of lattice distortion, grain refinement, and relaxor polarization dynamics are balanced without significant deterioration of field-induced polarization.

The developed design strategy may be extended to other lead-free relaxor ferroelectric systems intended for high-power pulse capacitors, power electronic modules, and advanced electrostatic energy-storage devices. Nevertheless, the present investigation was limited to quasi-static electrical characterization under laboratory conditions. Future work should focus on long-term charge–discharge cycling reliability, fatigue behavior, high-frequency pulse performance, thermal aging, and in situ structural characterization under applied electric fields to further elucidate the relationship between structural disorder and polarization dynamics.

References

[1] D. Li *et al.*, “Progress and perspectives in dielectric energy storage ceramics,” *J. Adv. Ceram. 2021 104*, vol. 10, no. 4, pp. 675–703, Jul. 2021, doi: 10.1007/S40145-021-0500-3.

[2] P. Zhao, Z. Cai, L. Wu, C. Zhu, L. Li, and X. Wang, “Perspectives and challenges for lead-free energy-storage multilayer ceramic capacitors,” *J. Adv. Ceram. 2021 106*, vol. 10, no. 6, pp. 1153–1193, Nov. 2021, doi: 10.1007/S40145-021-0516-8.

[3] Z. Yang, H. Du, L. Jin, and D. Poelman, “High-performance lead-free bulk ceramics for electrical energy storage applications: design strategies and challenges,” *J. Mater. Chem. A*, vol. 9, no. 34, pp. 18026–18085, Sep. 2021, doi: 10.1039/D1TA04504K.

[4] L. Wu *et al.*, “Enhanced energy-storage performance in BNT-based lead-free dielectric ceramics via introducing SrTi0.875Nb0.1O3,” *J. Mater.*, vol. 8, no. 3, pp. 537–544, May 2022, doi: 10.1016/J.JMAT.2022.01.003.

[5] A. Xie, J. Fu, and R. Zuo, “Achieving stable relaxor antiferroelectric P phase in NaNbO3-based lead-free ceramics for energy-storage applications,” *J. Mater.*, vol. 8, no. 3, pp. 618–626, May 2022, doi: 10.1016/J.JMAT.2021.11.012.

[6] Y. Zhang *et al.*, “Optimization of Energy Storage Properties in Lead-FreeBarium Titanate-Based Ceramics via

B-SiteDefect Dipole Engineering," *ACS Sustain. Chem. Eng.*, vol. 10, no. 9, pp. 2930–2937, Mar. 2022, doi: 10.1021/ACSSUSCHEMENG.1C07768.
[7] T. Pan *et al.*, "Enhanced Energy Density and Efficiency in Lead-Free Sodium Niobate-Based Relaxor Antiferroelectric Ceramics for Electrostatic Energy Storage Application," *Adv. Electron. Mater.*, vol. 8, no. 12, p. 2200793, Dec. 2022, doi: 10.1002/AELM.202200793;WGROUP:STRING:PUBLICATION.
[8] F. Yan *et al.*, "Boosting Energy Storage Performance of Lead-Free Ceramics via Layered Structure Optimization Strategy," *Small*, vol. 18, no. 34, p. 2202575, Aug. 2022, doi: 10.1002/SMLL.202202575;WGROUP:STRING:PUBLICATION.
[9] C. Zhu, Z. Cai, L. Guo, Y. Jiang, L. Li, and X. Wang, "SimultaneouslyAchieved Ultrastable Dielectric andEnergy Storage Properties in Lead-Free Bi0.5Na0.5TiO3-Based Ceramics," *ACS Appl. Energy Mater.*, vol. 5, no. 2, pp. 1560–1570, Feb. 2022, doi: 10.1021/ACSAEM.1C02964.
[10] A. Khan *et al.*, "Fabrication of a lead-free ternary ceramic system for high energy storage applications in dielectric capacitors," *Front. Chem.*, vol. 10, p. 1025030, Oct. 2022, doi: 10.3389/FCHEM.2022.1025030/TEXT.
[11] K. Yao *et al.*, "A new strategy to realize high energy storage properties and ultrafast discharge speed in Sr0.7Bi0.2TiO3-based relaxor ferroelectric ceramic," *J. Alloys Compd.*, vol. 883, p. 160855, Nov. 2021, doi: 10.1016/J.JALLCOM.2021.160855.
[12] R. L. Nayak, S. S. Dash, Y. Zhang, and M. P. K. Sahoo, "Enhanced dielectric, thermal stability, and energy storage properties in compositionally engineered lead-free ceramics at morphotropic phase boundary," *Ceram. Int.*, vol. 47, no. 12, pp. 17220–17233, Jun. 2021, doi: 10.1016/J.CERAMINT.2021.03.033.
[13] H. Yang, Z. Cai, C. Zhu, P. Feng, and X. Wang, "Ultra-High Energy Storage Performance in BNT-basedFerroelectric Ceramics with Simultaneously Enhanced Polarization andBreakdown Strength," *ACS Sustain. Chem. Eng.*, vol. 10, no. 28, pp. 9176–9183, Jul. 2022, doi: 10.1021/ACSSUSCHEMENG.2C02155.
[14] B. Guo *et al.*, "Energy storage performance of Na0.5Bi0.5TiO3 based lead-free ferroelectric ceramics prepared via non-uniform phase structure modification and rolling process," *Chem. Eng. J.*, vol. 420, p. 130475, Sep. 2021, doi: 10.1016/J.CEJ.2021.130475.
[15] R. Kang *et al.*, "DomainEngineered Lead-Free Ceramics with Large EnergyStorage Density and Ultra-High Efficiency under Low Electric Fields," *ACS Appl. Mater. Interfaces*, vol. 13, no. 21, pp. 25143–25152, Jun. 2021, doi: 10.1021/ACSAMI.1C05824.
[16] Y. Li *et al.*, "Improved electric energy storage properties of BT-SBT lead-free ceramics incorporating with A-site substitution with Na & Bi ions and liquid sintering generated by Na0.5Bi0.5TiO3," *J. Alloys Compd.*, vol. 856, p. 156708, Mar. 2021, doi: 10.1016/J.JALLCOM.2020.156708.

Information about authors:
Alexey Fedorov – PhD, Research Engineer, Electronic Ceramics Department, Jozef Stefan Institute, Ljubljana, Slovenia, alexey.fedorov@ijs.si

Author Contributions:
Alexey Fedorov – concept, methodology, resources, data collection, testing, modeling, analysis, visualization, interpretation, drafting, editing, funding acquisition.

Conflict of Interest: The authors declare no conflict of interest.

Use of Artificial Intelligence (AI): The authors declare that AI was not used.

Received: 09.07.2026
Revised: 11.09.2026
Accepted: 18.09.2026
Published: 28.09.2026